Human Cancer Biology

Clinical Cancer Research

Prevailing Role of Contact Guidance in Intrastromal T-cell Trapping in Human Pancreatic Cancer

Natalie Hartmann[1], Nathalia A. Giese[1], Thomas Giese[2], Isabel Poschke[3], Rienk Offringa[3], Jens Werner[1], and Eduard Ryschich[1]

Abstract

Purpose: Pancreatic ductal adenocarcinoma (PDAC) is characterized by extensive collagen-rich stroma. T cells that infiltrate pancreatic cancers frequently become trapped in the stroma and do not contact tumor cells. Here, we aimed to analyze how chemokines and extracellular matrix (ECM) collagen interact in mediating T-cell infiltration in PDAC.

Experimental Design: T-cell distribution and ECM structure within tumors were analyzed. Chemokine concentrations in human PDAC were compared with the levels of immune cell infiltration. We assessed the influences of selected chemokines and collagen on directed and random T-cell movement using *in vitro* migration systems.

Results: PDAC overproduced several T-cell-active chemokines, but their levels were not correlated with intratumoral T-cell infiltration. In the absence of collagen, directed migration of activated T cells was induced by chemokines. Interestingly, collagen itself promoted high migratory activity of T cells, but completely abolished chemokine-guided movement. This effect was not altered by a β_1-integrin blocking antibody. Activated T cells actively migrated in low-density collagen matrices, but migration was inhibited in dense collagen. Accordingly, T cells were heterogeneously distributed in the pancreatic cancer stroma, with the majority residing in areas of low-density collagen far from tumor clusters.

Conclusion: The excessive desmoplasia in PDAC promotes T-cell migration by contact guidance, which abrogates tumor cell–directed movement. Furthermore, dense collagen networks represent a physical barrier, additionally rearranging T-cell distribution to favor tumor stroma. These mechanisms are mainly responsible for intrastromal T-cell trapping in pancreatic cancer and may hinder the development of T-cell–based immunotherapies. *Clin Cancer Res; 20(13); 3422–33. ©2014 AACR.*

Introduction

Pancreatic ductal adenocarcinoma (PDAC), one of the most common causes of cancer death worldwide, is usually diagnosed at an advanced stage and has an overall 5-year survival rate of below 5% (1). The poor outcomes of PDAC reflect our current limited understanding of this complex and highly aggressive tumor. There is an urgent need for the development of new treatment strategies, such as immunotherapeutic approaches.

The tumor microenvironment plays a decisive role in tumor defense and progression. In PDAC, the stroma is composed of multiple cell types, including fibroblasts, pancreatic stellate cells (PSC), endothelial cells, and inflammatory cells, which secrete a variety of factors, such as extracellular matrix (ECM) components, cytokines, and chemokines (2). Collagen type I is the most abundant ECM protein in PDAC (3–5). PDAC is characterized by particularly strong desmoplasia, with the stromal fraction often exceeding the epithelial portion of the tumor, which is considered an important factor driving tumor progression and mediating chemotherapy resistance (2). Recent studies in mice show stromal depletion resulting in sensitization of PDAC to chemotherapeutic intervention (6–8).

The degree of T-cell infiltration has been identified as an important prognostic factor in various types of cancer. Strong infiltration, especially by cytotoxic $CD8^+$ T cells, is usually associated with improved patient outcomes (9, 10). Human PDAC frequently induces an immune response resulting in marked T-cell infiltration (11, 12). However, the vast majority of tumor-infiltrating T cells become trapped in the stroma and peritumoral tissue by some yet unknown mechanism, and thus the T cells do not reach the cancer cells in sufficient numbers (12, 13).

Authors' Affiliations: Departments of [1]General Surgery and [2]Immunology, University of Heidelberg; and [3]Department of Translational Cancer Research, German Cancer Research Center, Heidelberg, Germany

Note: Supplementary data for this article are available at Clinical Cancer Research Online (http://clincancerres.aacrjournals.org/).

Corresponding Author: Eduard Ryschich, Department of General Surgery, University of Heidelberg, Im Neuenheimer Feld 365, 69120 Heidelberg, Germany. Phone: 49-6221-56-6110; Fax: 49-6221-56-4208; E-mail: eduard.ryschich@med.uni-heidelberg.de

doi: 10.1158/1078-0432.CCR-13-2972

Translational Relevance

Extensive desmoplasia is an important feature of PDAC, which contributes to its therapy resistance. PDACs are infiltrated by T cells that predominantly become trapped in the stroma and thus fail to reach the tumor. The present study demonstrates that the prevailing force of contact guidance supports stromal accumulation of T cells by abrogating intratumoral chemokine-guided T-cell migration and misdirecting them away from tumor cells. As the predominant stromal component in PDAC, collagen type I may additionally form a physical barrier that limits T cell access to tumor cells. Misguidance of T cells by tumor stroma may impede antitumoral immune responses, thus contributing to the poor prognosis of this malignant disease. The strong desmoplastic reaction in pancreatic cancer may suppress or block the efficacy of T-cell–based strategies, including adoptive transfer and antibody treatment. Furthermore, matrix-degrading treatment approaches might significantly improve the efficacy of endogenous antitumor immune responses and T-cell–based immunotherapies.

T-cell migration into and within tumors is guided by chemokines and ECM proteins (14, 15). Several of the most important chemokines in this process include stromal cell-derived factor-1 (SDF-1; CXCL12), IFNγ-inducible protein 10 (IP-10; CXCL10), and macrophage inflammatory protein-1β (MIP-1β; CCL4) along with their corresponding chemokine receptors: CXC chemokine receptor (CXCR) 4, CXCR3, and CC chemokine receptor (CCR) 5 (16–18). In particular, CXCR3 and CCR5 are important mediators of T-cell homing to sites of inflammation (19). These and other CRs have been implicated in T-cell recruitment into a variety of cancer entities, and the corresponding chemokines are often overexpressed (14, 20–22). Two types of directed T-cell movement have been identified: chemotaxis, which is induced by soluble, freely diffusing compounds, and haptotaxis, which is cell migration toward a concentration gradient of ECM-bound chemokine (15).

In addition to chemokine-induced migration, T cells move through the three-dimensional (3D) ECM by contact guidance, which is described as migration along ECM fibers and squeezing through matrix gaps, following the path of least resistance (15). In contrast with migration across two-dimensional ECM, which requires interactions between leukocyte integrins and the substrate, contact guidance is an amoeboid-like type of migration that is usually independent of integrins and matrix-metalloproteinases (15, 23, 24). ECM structures can provide a scaffold that supports 3D T-cell migration, but dense ECM fiber alignment can create nonpermissive matrix regions that exclude T cells. Several studies have demonstrated such nonpermissive stromal areas in human tumors, which may complicate antitumor immune responses (25–27). Here, we investigated the mechanisms controlling intratumoral T-cell migration in PDAC in terms of chemokines and contact guidance, and determined whether and how these mechanisms contribute to immune evasion of PDAC.

Materials and Methods

Patients and tissue samples

This study included patients undergoing surgery for pancreatic carcinoma in the Department of Surgery at the University of Heidelberg (Heidelberg, Germany). The protocol was approved by the local ethics committee, and informed consent was obtained from all patients, in accordance with the Helsinki declaration. Normal pancreatic specimens were obtained from donor organs in cases where no suitable recipient was found through the Eurotransplant program. Tissue samples were snap-frozen and stored in liquid nitrogen.

Cell culture and T-cell activation

Cell lines were grown in complete RPMI-1640 (cc-pro) supplemented with 10% fetal calf serum (FCS; PAA), 2 mmol/L L-glutamine, 20 U/mL penicillin, and 0.1 mg/mL streptomycin (cc-pro). For T-cell culture, we added 1 mmol/L sodium pyruvate (Biochrom AG) and 0.05 mmol/L β-mercaptoethanol (Gibco). Boyden chamber assays were performed in phenol red-free RPMI-1640 (cc-pro) supplemented with 0.5% or 1% FCS (PAA), 0.2% cell culture-tested bovine serum albumin (Sigma-Aldrich), 2 mmol/L L-glutamine, 20 U/mL penicillin, 0.1 mg/mL streptomycin (cc-pro), 1 mmol/L sodium pyruvate (Biochrom AG), and 0.05 mmol/L β-mercaptoethanol (Gibco). Cell cultures were incubated at 37°C in a humidified atmosphere with 5% CO_2.

Peripheral blood mononuclear cells (PBMC) were isolated from healthy donors by density gradient centrifugation using Biocoll (Biochrom AG). From these PBMCs, we isolated unstimulated T cells by magnetic-activated cell sorting using CD3 Microbeads and LS columns (Miltenyi Biotech) following the manufacturer's instructions. For activation, PBMCs were stimulated for 24 hours with 12.5 μg/mL concanavalin A (Calbiochem) or for 48 hours with 3 μg/mL plate-bound anti-CD3 (clone OKT3) and 1 μg/mL plate-bound anti-CD28 (clone CD28.2; eBioscience). The cells were next cultured for 5 to 7 days in the presence of 50 U/mL interleukin-2 (IL-2; PeproTech). The percentage of $CD3^+$ cells was determined by flow cytometry, and was >95% in all samples.

Single-cell suspensions were obtained from tumor tissues by scratching the tissue surface with a scalpel and passing the suspension through a 70-μmol/L cell strainer (BD Falcon). The cells were immediately analyzed by flow cytometry. For *in vitro* migration assays, T cells were extracted from tumors by incubating tissue pieces in high-dose IL-2 (6000 U/mL). The cells were subsequently expanded in the presence of 30 ng/mL anti-CD3 antibody (clone OKT3; eBioscience) and a mixture of allogeneic PBMCs from three donors, which had been inactivated by an irradiation dose of 40 Gy.

Analysis of tissue chemokine levels

Chemokine and CR mRNA levels in total tissue lysates were determined by quantitative real-time PCR (qRT-PCR) as described previously (28, 29). All materials and equipment for RNA and cDNA preparation were obtained from Roche and used following the manufacturer's instructions. Target-specific and housekeeping gene cyclophilin B (CPB)-specific primers were purchased from Search LC.

To determine chemokine protein levels, snap-frozen tissue was cut into 50 μmol/L cryosections, and homogenized using the Bioplex Cell Lysis Kit (BioRad) following the manufacturer's instructions. Chemokine concentrations were then assessed using Bioplex technology (BioRad) according to the manufacturer's instructions.

Immunohistochemistry, immunofluorescence, and second harmonic generation microscopy

For immunohistochemistry, 7 μm acetone-fixed cryosections were stained overnight at 4°C with antibodies against CD3 (clone F7.2.38; Dako), CXCR4 (clone 44716; R&D Systems), CXCR3 (polyclonal; Acris), or CCR5 (clone eBioT21/8; eBioscience) or with the corresponding isotype controls in TBS with 1% BSA. Immune complexes were developed using the LSAB$^+$ detection system (Dako) according to the manufacturer's instructions. Sections were counterstained with hematoxylin (Roth) and analyzed under a Leica DMRB bright-field microscope (Leica). In the same samples used for Bioplex analysis ($n = 29$), we assessed the densities of CD3$^+$ and CR-expressing cells by direct leukocyte counting in three random microscopic fields (total area: 0.27 mm^2). These results were expressed using the following scale: 0 = absent, 1 = low, 2 = moderate, 3 = high, and 4 = very high infiltration. In 100 tumor samples, we determined maximum CD3$^+$ infiltration (Fig. 1A) by identifying the microscopic areas with maximum T-cell accumulation and grading the T-cell infiltration in these areas using the above scale, as described previously (13, 30).

For laser-scanning confocal microscopy (LSCM), cryosections from three tumor samples were fixed with acetone, and then stained with antibodies against collagen type I (polyclonal; Acris) and cytokeratin-7 (clone OV-TL 12/30; Zytomed), followed by anti-rabbit–DyLight649 (BioLegend) and anti-mouse–DyLight550 (Biomol), and finally with anti-CD3–AlexaFluor488 (clone HIT3a; BioLegend), each for 1 hour at room temperature. Sections were counterstained with 4′, 6-diamidino-2-phenylindole and analyzed using an A1R confocal microscope (Nikon).

For second harmonic generation (SHG) microscopy, cryosections from seven tumor samples were fixed with 20 μmol/L 4% paraformaldehyde. These sections were then stained for 5 hours with an antibody against cytokeratin-7 (clone OV-TL 12/30; Zytomed), followed by anti-mouse–AlexaFluor568 (Invitrogen) for 5 hours, and finally with anti-CD3–AF488 (clone HIT3a; BioLegend) overnight at 4°C. Fluorescence and collagen SHG signals were detected using a TriM Scope 2-photon microscope (LaVision).

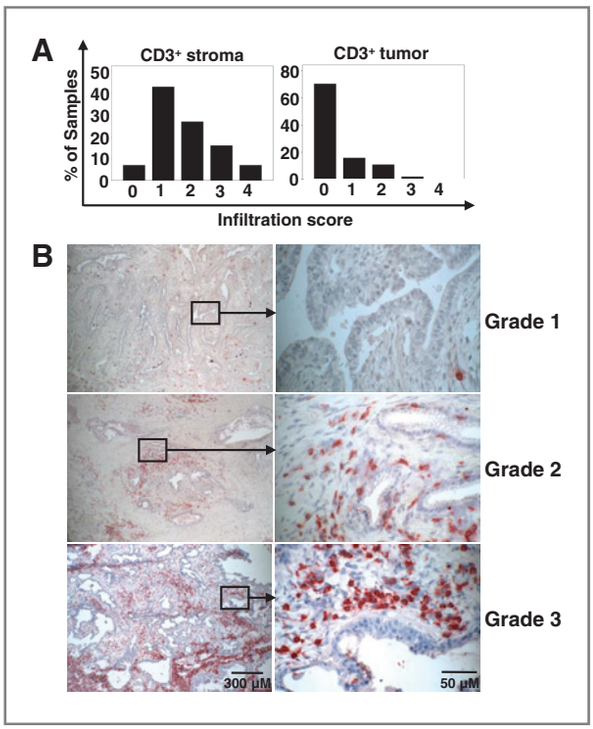

Figure 1. PDAC-infiltrating T cells mainly accumulate in the tumor stroma, and rarely contact tumor cells. A, quantitative analysis of intratumoral CD3$^+$ T-cell infiltration in human PDAC: 0 = absent, 1 = low, 2 = moderate, 3 = high, and 4 = very high infiltration. Almost 50% of tumor samples showed moderate or higher infiltration ($n = 100$). B, representative images of immunohistochemistry showing different grades of stromal CD3$^+$ infiltration.

Flow cytometry

Cells (2×10^5/sample) were stained for 30 minutes in PBS containing 0.1% BSA, 0.05% sodium azide, and fluorescent dye-conjugated antibodies against CD3 (clone OKT3), CD4 (clone SK3), CD8 (clone OKT8), CD45RO (clone UCHL1), CCR7 (clone 3D12), CXCR4 (clone 12G5), CD49b (clone eBioY418; all purchased from eBioscience), CD29 (clone TS2/16; BioLegend), CCR5 (clone 45531; R&D Systems), and CXCR3 (clone 1C6; BD Biosciences) or the corresponding isotype controls. Dead cells were excluded by 7-aminoactinomycin D staining (Sigma-Aldrich). Data were acquired on an LSR II flow cytometer (Beckton Dickinson) and analyzed using FlowJo software (Tree Star).

Migration systems

For Boyden chamber assays, cells were serum-starved overnight at 37°C in medium containing 0.5% FCS. Cells (2×10^6/mL) were labeled with 4 μmol/L calcein AM (Santa Cruz Biotechnology) for 1 hour at 37°C. The cells and chemokine solutions were prepared in serum-reduced medium (1% FCS). Cells (1×10^4/well) were seeded in the upper wells of HTS Transwell-96 plates (Corning). Migration was induced with 100 ng/mL SDF-1 or IP-10 (PeproTech). After 3 hours, migration was measured as

fluorescence intensity in the lower wells using a FLUOstar OPTIMA imager (BMG Labtech). Where indicated, the upper wells were coated with 0.1 mg/mL collagen type I (Serva) for 3 hours at 37°C, and then dried overnight at room temperature.

For 3D migration at uniform chemokine distribution, a collagen type I solution (Serva) was used to produce collagen matrices of varying density with or without added chemokine (SDF-1 or IP-10, 100 ng/mL). These matrices were allowed to polymerize in 96-well flat-bottom plates for 45 minutes at 37°C in a humidified chamber. Cells in PBS were then seeded at a density of 1×10^5/well on the gels, and examined using an Axio Observer.Z1 bright-field microscope (Zeiss). Migration was assessed by measuring the z-distance from the top of the gel to the migration front after 3 hours, or by counting the cells at $\Delta z = 1$ mm after 12 hours.

For 3D migration in the presence of a chemokine gradient, cells (9×10^6/mL) were seeded in 1 mg/mL collagen type I gels in a μ-slide chemotaxis 3D (Ibidi) following the manufacturer's instructions. The cells were then exposed to gradients of SDF-1 or IP-10 (maximum: 100 ng/mL). Migration was recorded once per minute for 1 hour by time-lapse microscopy using an Axio Observer.Z1 bright-field microscope (Zeiss). A constant temperature of 37°C and constant 5% CO_2 level were ensured using heatable incubation chambers and temperature/CO_2 control units (Pecon). The percentage of migrating cells was determined and directional migration was analyzed by manually tracking 20 individual cells per condition and calculating the percentage of cells oriented toward the chemokine. As an additional measure of directional migration, the mean chemotropism index (MCI) was calculated according to Tharp and colleagues (31).

To analyze the ability of collagen to bind chemokines, 100 ng/mL of SDF-1 or IL-10 was added to 100 μL of collagen matrix mixture before polymerization. After polymerization, 100 μL PBS was added on the matrix. ELISA was used to measure the concentration of nonbound chemokine released into the PBS over 5 hours at 37°C. The same chemokine solution in PBS without matrix was used as a reference.

For some experiments, 1×10^6 fluorescently labeled T cells were pretreated with 5 μg anti–β_1-integrin blocking antibody (clone 6S6; Millipore) for 15 minutes at 37°C. A FLUOstar OPTIMA fluorimeter (BMG Labtech) was used to determine blocking efficiency of cell attachment to collagen-coated plates (15 minutes at 37°C) before and after treatment. The same method was utilized to measure attachment of T cells to collagen-coated plates that were pretreated with 100 ng/mL of SDF-1 or IP-10 for 30 minutes at 37°C ($n = 3$).

Statistical analysis

The Mann–Whitney test was used to determine the statistical significance for qRT-PCR and Bioplex data. Migration data were compared by ANOVA. $P < 0.05$ was considered to be significant.

Results

PDAC-infiltrating T cells mainly accumulate in the tumor stroma and express the CRs CXCR3, CXCR4, and CCR5

T-cell infiltration and distribution in PDAC tissue were studied by immunohistochemistry. Approximately 50% of the tumor samples were not or rarely infiltrated by $CD3^+$ cells (grade 0–1), whereas the other half showed marked infiltration (grade 2–4). T cells were mainly localized in the tumor stroma and rarely contacted tumor cells (Fig. 1A and B).

Next, qRT-PCR was used to analyze the expressions of CRs related to T-cell homing. In tumor tissue compared with in normal pancreas samples, CXCR4 and CXCR3 mRNA levels were increased by 19- and 25-fold, respectively, ($P < 0.001$), whereas CCR5 mRNA levels did not significantly differ between groups (Fig. 2A). Flow-cytometric analysis of the activation status and CR profile of PDAC-infiltrating T cells revealed that, immediately after isolation or after *in vitro* expansion, tumor-derived T cells displayed an effector/memory phenotype ($CD45RO^+$ $CCR7^-$) and mainly expressed the CRs CXCR4 and CXCR3 and, to some extent, CCR5 (Fig. 2B and C). This phenotype was mimicked in peripheral blood-derived T cells (PBT) by standard activation protocols (Supplementary Fig. S1A and S1B).

Chemokine levels are dysregulated in PDAC, but do not correlate with T-cell infiltration

Next, production of the corresponding T-cell-active chemokines, SDF-1, IP-10, and MIP-1β, was assessed using qRT-PCR and Bioplex technology. All three chemokines were expressed in both normal pancreas and pancreatic cancer samples. In tumors compared with in nonmalignant tissue, IP-10 mRNA ($P < 0.001$) and MIP-1β mRNA ($P = 0.002$) expressions were upregulated by 9- and 15-fold, respectively, whereas SDF-1 mRNA expression was unchanged (Fig. 3A). At the protein level, IP-10 and MIP-1β were overexpressed in tumor tissue by 40- and 10-fold, respectively, ($P < 0.001$). Interestingly, SDF-1 protein was also upregulated by 2-fold ($P = 0.022$) in tumors compared with nonmalignant tissue (Fig. 3B). However, immunohistochemical quantification of tumor-infiltrating $CD3^+$ and CR-expressing cells revealed no correlations with the chemokine concentrations measured in the corresponding samples (Fig. 3C and D). Because CXCR4 and CXCR3 were elevated at the mRNA level and were predominantly expressed in tumor-infiltrating T cells, their corresponding ligands (SDF-1 and IP-10) were selected for T-cell migration studies.

Collagen matrices promote T-cell migration by contact guidance that abrogates chemokine-guided migration

To clarify whether contact guidance was an important determinant of T-cell migration in PDAC, we tested the chemotactic responses of activated T cells in the presence or absence of collagen type I. Activated PBTs responded well to SDF-1 and IP-10 in a Boyden chamber ($P \leq 0.001$

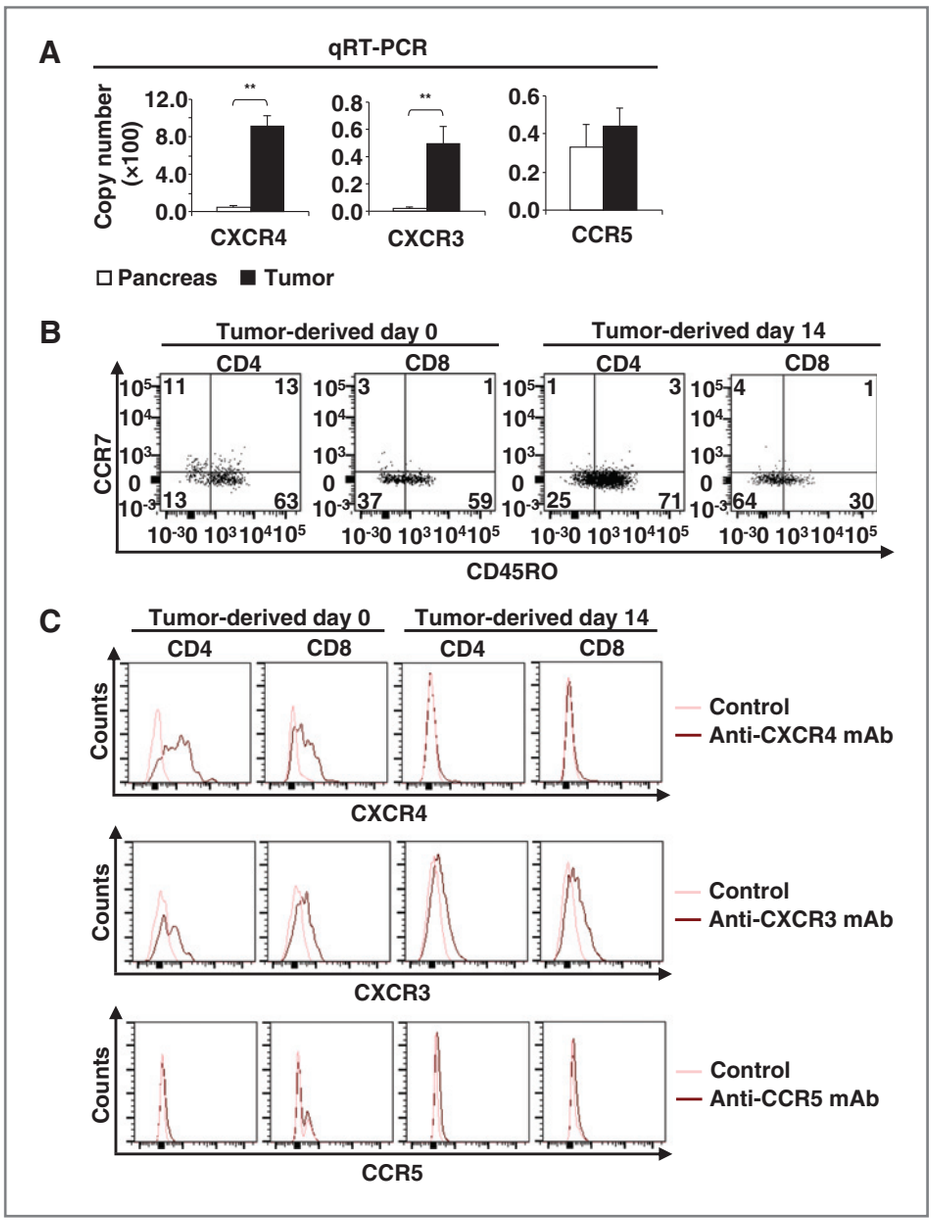

Figure 2. PDAC-infiltrating T cells express CXCR3, CXCR4, and CCR5. A, comparison of CR expression in normal pancreas (NP) and tumors (T) by qRT-PCR. Data are shown as the mean target copy numbers and SEM per 10,000 copies of the housekeeping gene CPB. CXCR4: $n = 37$ (NP), $n = 61$ (T); CXCR3: $n = 22$ (NP), $n = 39$ (T); CCR5: $n = 4$ (NP), $n = 6$ (T). **, $P < 0.001$. Tumors showed higher expressions of CXCR4 and CXCR3. B and C, flow-cytometric analysis of T-cell phenotype (B) and CR expression (C) in freshly isolated (day 0) and cultured (day 14) tumor-derived T cells. Light red lines represent the isotype control, and dark red lines represent specific staining. Tumor-derived T cells displayed an effector/memory phenotype ($CD45RO^+$ $CCR7^-$) and mainly expressed the CRs CXCR4 and CXCR3 and, to some extent, CCR5. Representative samples are shown (total $n = 3$).

for medium alone vs. with SDF-1 or IP-10). Interestingly, this effect was completely abrogated when the membrane was coated with collagen type I ($P < 0.001$; Fig. 4A). We next examined chemokine-induced T-cell migration in a collagen matrix using time-lapse microscopy. Without chemokines, nonactivated PBTs displayed low migrational activity, which was strongly increased upon exposure to a gradient of SDF-1 ($P = 0.015$), but not IP-10 (Fig. 4B). This observation corresponded to nonactivated PBTs displaying high surface expression of CXCR4, whereas CXCR3 expression was absent in this subpopulation (Supplementary Fig. S1B). Nonactivated PBTs showed directional migration toward SDF-1 (MCI = +0.16; $P = 0.04$ for medium alone vs. SDF-1), but not IP-10 (MCI = −0.08; $P = 0.656$ for medium alone vs. IP-10). Activated PBTs and tumor-derived T cells showed higher basal migration in collagen matrices, which was not further enhanced by gradients of SDF-1 or IP-10 (Fig. 4B), despite CR expression (Fig. 2C and Supplementary Fig. S1B). Activated PBTs and tumor-derived T cells migrated in a random, chemokine-independent manner ($0.1 > MCI > -0.1$ in all cases; Fig. 4E).

To differentiate between effects of the bound (haptotaxis) and soluble (chemotaxis) chemokine fractions, we studied the binding capacity of chemokines to collagen and their influence on T-cell adhesion. SDF-1 showed a high capacity to bind to collagen matrix during polymerization, although a fraction of SDF-1 remained unbound and was released

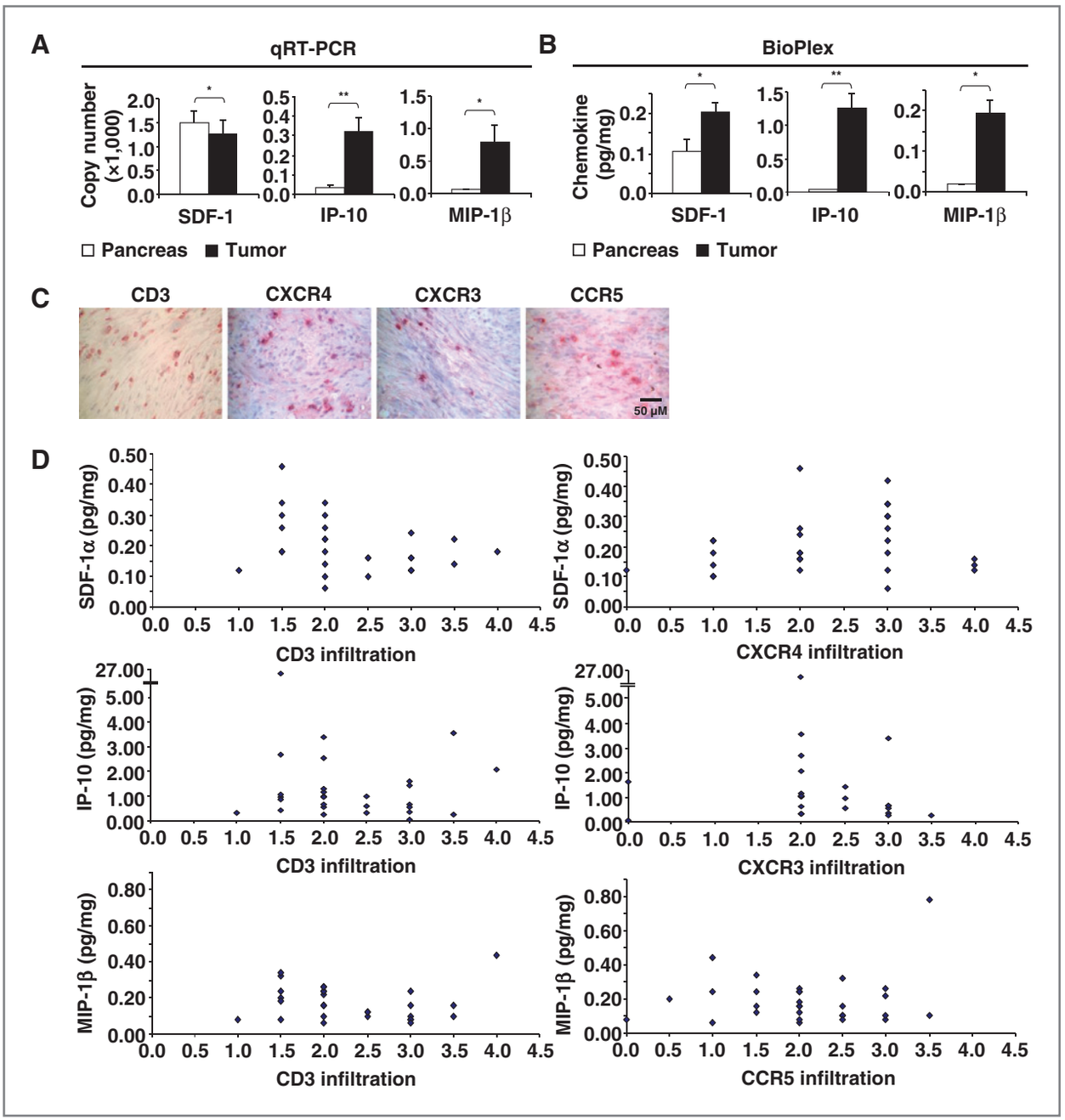

Figure 3. Chemokine levels are dysregulated in PDAC, but do not correlate with T-cell infiltration. A and B, chemokine expression compared between normal pancreas (NP) and tumors (T) at the mRNA level by qRT-PCR (A), and at the protein level using Bioplex technology (B). A, data are shown as mean target copy numbers and SEM per 10,000 copies of the housekeeping gene CPB. SDF-1: $n = 39$ (NP), $n = 61$ (T); IP-10: $n = 24$ (NP), $n = 31$ (T); MIP-1β: $n = 11$ (NP), $n = 5$ (T). **, $P < 0.001$. B, data are shown as the amount of chemokine/total protein and SEM. $n = 5$ (NP), $n = 29$ (T). *, $P < 0.05$; **, $P < 0.001$. C, representative images of immunohistochemical analysis of $CD3^+$ and CR expression in cells from tumor samples. D, quantitative analysis of infiltration by $CD3^+$, $CXCR4^+$, $CXCR3^+$, and $CCR5^+$ cells ($n = 29$ samples) and comparison with the chemokine levels in the corresponding patients. Infiltration grades: 0 = absent, 1 = low, 2 = moderate, 3 = high, and 4 = very high infiltration.

into the soluble phase (Fig. 4C). IP-10 showed no binding to collagen (Fig. 4C). Furthermore, T-cell adhesion to collagen-coated plates was not increased after pretreatment with SDF-1 or IP-10 (Fig. 4D).

Contact guidance migration of activated T cells is independent of β_1-integrin

$\alpha_2\beta_1$-integrin was expressed on nonactivated PBTs and upregulated after activation. It was also present on freshly

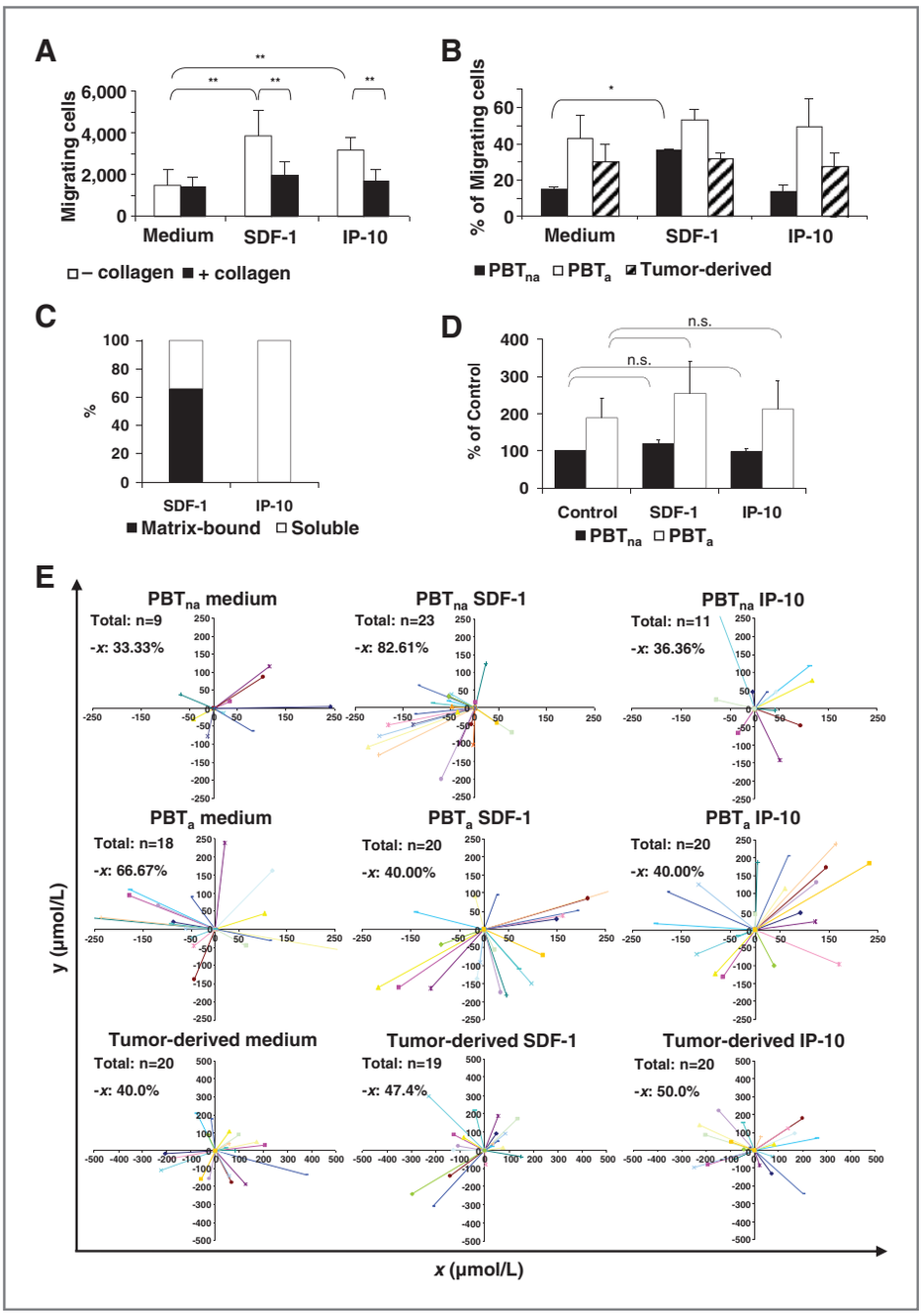

Figure 4. Collagen matrices promote T-cell migration by contact guidance, thus abrogating chemokine-induced migration. A, migration of activated PBTs in a Boyden chamber in response to SDF-1 or IP-10 with or without collagen type I coating. Data presented as the mean and SD of three independent experiments. *, $P < 0.05$; **, $P \leq 0.001$. B, migrational activity of nonactivated PBTs, activated PBTs, and tumor-derived T cells in a collagen type I matrix in the presence of a chemokine gradient. The percentage of migrating cells/total cells is shown. Data are presented as the mean and SD of two to three independent experiments. *, $P < 0.05$. C, binding of SDF-1 and IP-10 to collagen matrix during matrix polymerization. SDF-1 was partially bound, whereas IP-10 was not bound ($n = 3$). D, adhesion of T cells to a collagen-coated surface that was pretreated with chemokines. No significant differences were found ($P > 0.05$, $n = 3$). Data are shown as percent related to the nontreated PBT_{na} and SD of three independent experiments performed in triplicate. E, determination of directional migration of nonactivated PBTs, activated PBTs, and tumor-derived T cells in a collagen type I matrix with a chemokine gradient. Colored lines represent individual cells. The percentage of cells oriented toward the chemokine-containing chamber (= −×) of one representative experiment ($n = 2$–3) is indicated.

isolated and *in vitro* expanded tumor-derived T cells (Fig. 5A). Adhesion of untreated activated PBTs and tumor-derived T cells was 2- to 3-fold stronger than that of nonactivated PBTs. Blocking β_1-integrin reduced the adhesion of activated PBTs and tumor-derived T cells almost to the level of nonactivated PBTs ($P < 0.001$; Fig. 5B). Despite this rather strong effect on adhesion, β_1-integrin inhibition did not enhance basal migration or restore the activated T-cell response to chemokines in the presence of collagen type I in the Boyden chamber (Fig. 5C). Similarly, activated PBT migration in a collagen type I matrix was indistinguishable in the presence or absence of a uniform chemokine concentration, which was independent of β_1-integrin blockade (Supplementary Fig. S2). Total 3D migration of activated PBTs and tumor-derived T cells in the presence of a chemokine gradient was also unaltered upon treatment with the β_1-integrin antagonist (Fig. 5D). Moreover, there was no significant effect on the directional migration of activated T cells (0.1 > MCI > −0.1 in all cases; Fig. 5E).

High-density collagen networks impede T cell–tumor cell contact in PDAC

We next analyzed intratumoral T-cell localization relative to the local matrix density using LSCM (Fig. 6A) and SHG microscopy (Fig. 6B and C). Collagen type I was ubiquitously present in the tumor stroma (Fig. 6A). The stromal collagen fiber density was heterogeneous, but significantly higher near tumor cell clusters (Fig. 6C). Notably, T cells preferentially accumulated in areas of low collagen density. To confirm the impact of the collagen structure on T-cell migration *in vitro*, we examined the efficiency of T-cell invasion into 3D collagen matrices of different densities. Maximum invasion occurred at the lowest collagen density (0.5 mg/mL). The migration distance and numbers of invading T cells were significantly reduced with increasing matrix density, and the highest collagen density (1.5 mg/mL) almost completely suppressed invasion (Fig. 6D).

Discussion

In the initial part of the present study, the T-cell distribution in pancreatic tumors was analyzed and assigned to tumor clusters or stromal compartments. Half of the tumor samples showed moderate or high T-cell infiltration. Of these samples, all exhibited stromal infiltration, whereas only 28% exhibited moderate T-cell numbers within tumor clusters. These results suggested that the stroma in PDAC might play an important role in guiding infiltrating T cells, which was investigated further.

We examined two mechanisms that potentially determine intratumoral T-cell localization: chemokine-induced migration and contact guidance. We found that several T-cell-specific chemokines were strongly overproduced in PDAC. However, we observed no relationship between chemokine levels and the degree of infiltration by T cells or CR-expressing cells, demonstrating a circumstantial role of chemokines in T-cell infiltration of PDAC.

Next, we investigated the differential effects of chemokines and collagen type I on T-cell migration in detail using various migration systems. Our results clearly demonstrated that collagen promoted T-cell migration by contact guidance, which strongly prevailed over chemokine-induced responses. This effect was attributable to activated T cells, but not nonactivated T cells. Physiologically, these findings imply that the immune system produces functionally mature activated T cells expressing appropriate CRs, which are recruited to tumor sites, emigrate into tumor tissue from blood vessels, and are theoretically able to follow chemokine gradients. However, upon emigration, activated T cells contact the dense matrix of the pancreatic stroma, which switches their migrational mode from chemokine- to stroma-guided movement, thus misdirecting them from their migration toward tumor cells. Interestingly, SDF-1 can be bound by collagen matrix and may use both hapto- and chemotactic signals, whereas IP-10 does not bind to collagen and may act as chemotactic agent. The above results demonstrate that the prevalence of matrix-guided migration over chemokine action is independent from the mode of chemokine-induced migration, such as haptotaxis or chemotaxis.

One potential molecular mechanism for controlling T-cell migration through collagen in PDAC may involve $\alpha_2\beta_1$-integrin, which reportedly mediates T-cell adhesion to collagen (32). We found that both nonactivated and activated T cells expressed $\alpha_2\beta_1$-integrin, but only activated T cells efficiently adhered to collagen type I. This phenomenon may occur because integrins must switch to an active conformation to mediate adhesion, which can be induced by T-cell activation and chemokine exposure (33). β_1-integrin blockade efficiently reduced the adhesion of activated T cells to collagen-coated surfaces to the level observed in nonactivated T cells; however, it did not restore their chemokine responsiveness in a collagen matrix. This observation is in line with results from human lung tumors, in which β_1-integrin blockade alters the migration of activated T cells on two-dimensional surfaces, but not in a 3D matrix (27). The ability of T cells to migrate through the ECM in an integrin-independent manner has been described previously (23). Our findings indicate that activated T-cell migration in collagen matrices occurs predominantly in a β_1-integrin–independent manner. Furthermore, they suggest that integrin-mediated adhesion to collagen is not the major factor determining the nonresponsiveness of activated T cells to chemokines in the presence of collagen. Although our present findings did not identify any additional molecular mechanisms of contact guidance by collagen, it has been previously described that contact guidance may involve low adhesive interactions between T cells and collagen (15).

The principle of contact guidance is that matrix fiber orientation and density provide a scaffold along which T cells can migrate, following the path of least resistance (15). This behavior is feasible because T-cell migration in the ECM occurs independently of matrix-degrading mechanisms (34). Furthermore, it has been demonstrated that T cells are less potent than neutrophils in migrating through dense ECM networks because of their limited capacity for nuclear deformation (35). The present study demonstrates that this principle can be applied to describe T-cell migration in PDAC. *In vitro*, the extent of T-cell invasion into a collagen matrix was negatively correlated with the matrix density. This observation corresponds well with our data from tumor samples, which showed preferential T-cell accumulation in stromal areas of lower collagen density. Similar findings were previously reported in a study of human lung cancer, demonstrating that T cells preferentially localize to regions of low matrix density and display decreased motility in dense matrix areas (27). Those authors concluded that increased collagen deposition around tumor clusters may act as a substantial mechanical barrier for T cells. However, our present findings only partially support these conclusions, as the collagen shield around tumor cell clusters is highly discontinuous, and there was only a slightly difference in collagen density between the tumor cell surroundings and T-cell areas.

A dense ECM is a major hindrance in chemotherapeutic treatment of pancreatic cancer. Recent studies have demonstrated that the therapeutic resistance of PDAC can be

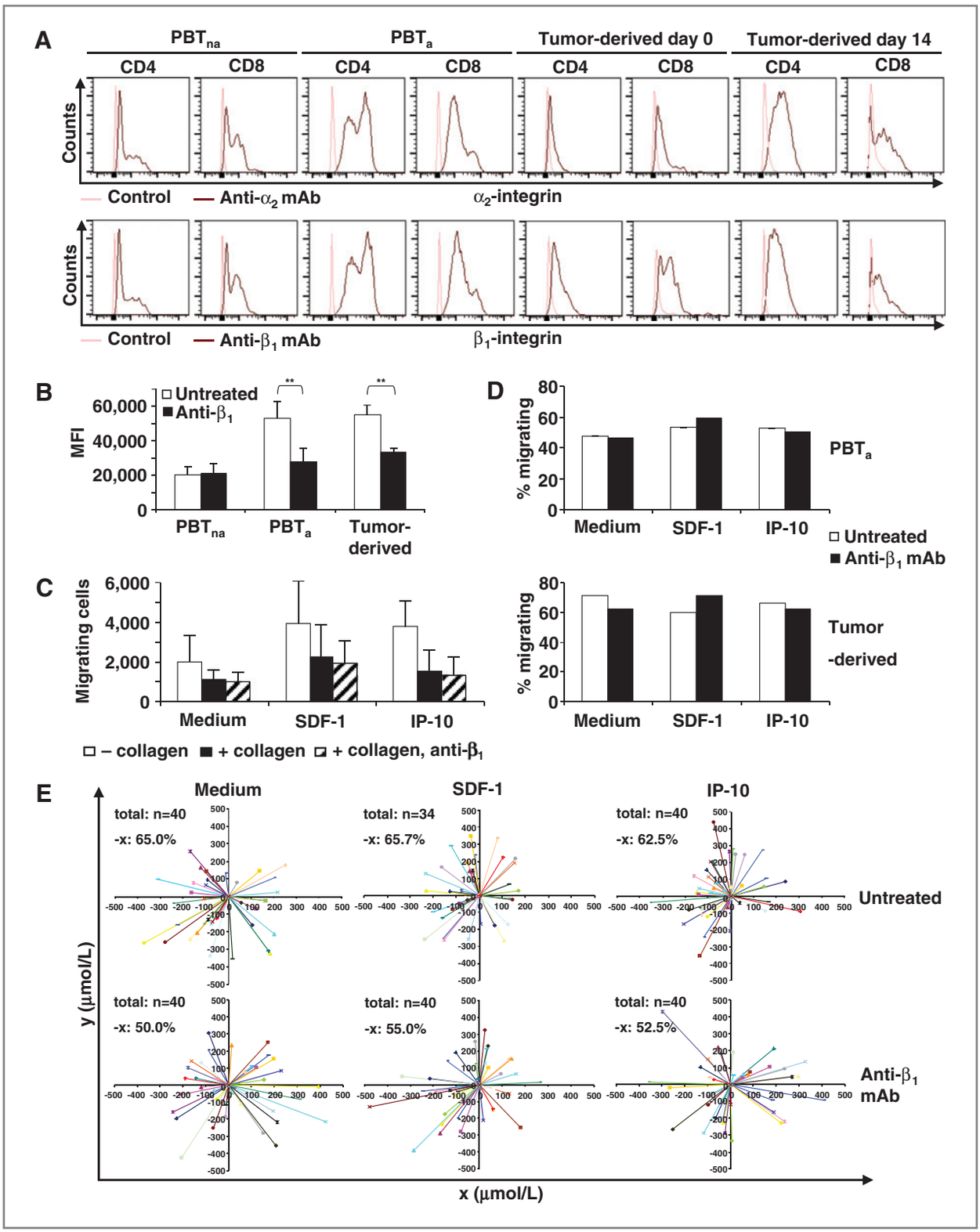

Figure 5. Contact guidance migration of activated T cells is independent of β_1-integrin. A, flow-cytometric analysis of $\alpha_2\beta_1$-integrin expression in nonactivated PBTs, activated PBTs, and freshly isolated (day 0) and cultured (day 14) tumor-derived T cells. Light red lines represent the isotype control, and dark red lines represent specific staining. Representative samples are shown (total $n = 3$). B, adhesion of nonactivated PBTs, activated PBTs, and tumor-derived T cells to a collagen type I–coated surface with or without treatment with an anti–β_1-integrin blocking monoclonal antibody (mAb). (*Continued on the following page.*)

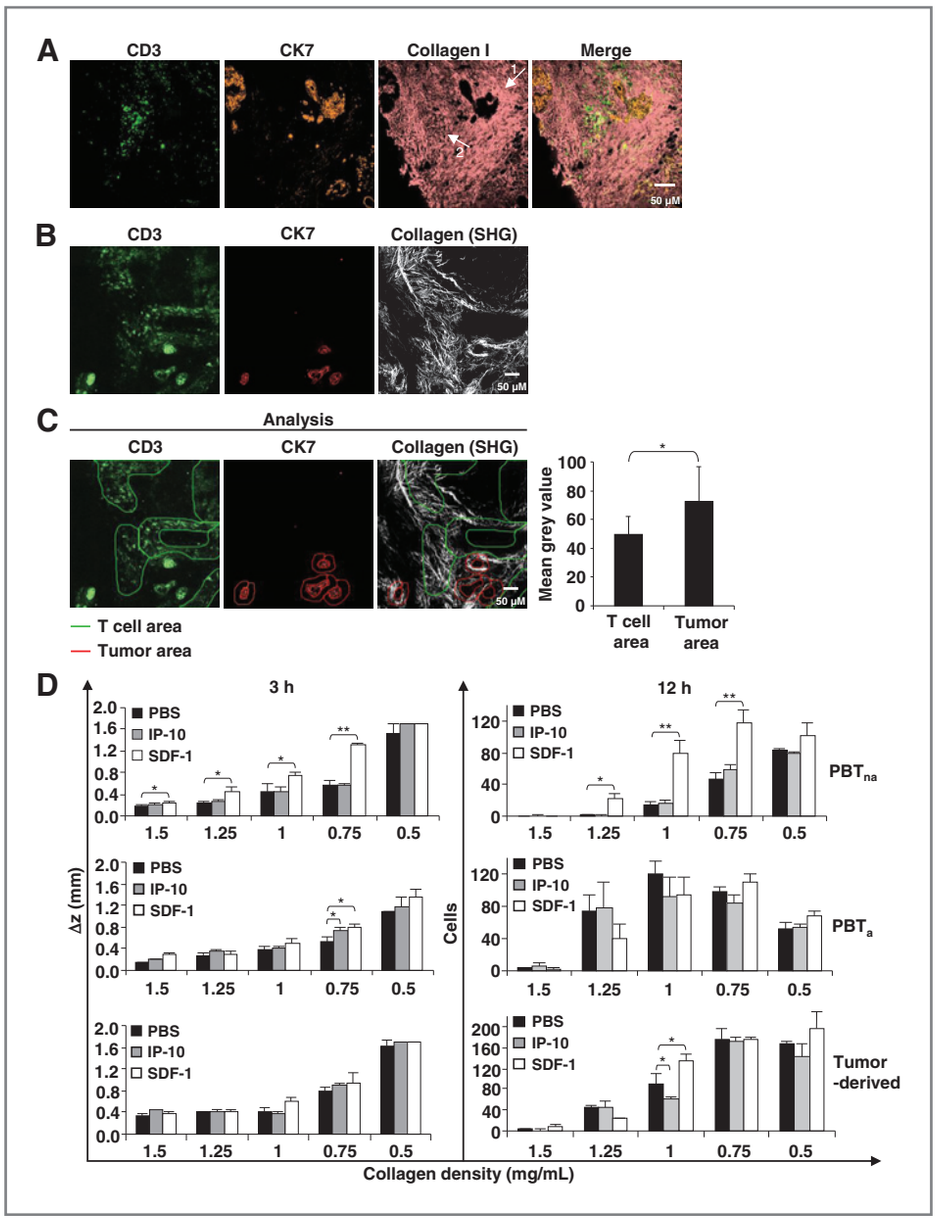

Figure 6. High-density collagen networks impede T cell–tumor cell contact in PDAC. A, representative images of LSCM. Arrow 1 indicates an area of densely packed collagen around a tumor cluster. Arrow 2 indicates loosely arranged collagen structures in the T-cell area. B, representative images of SHG microscopy. C, quantitative comparison of collagen density in tumor versus T-cell areas. Data shown as the mean gray values and SD. $P < 0.05$. D, migrational activity of nonactivated PBTs, activated PBTs, and tumor-derived T cells in collagen type I matrices of various densities (0.5–1.5 mg/mL) with uniform chemokine concentrations. Data show the distance (Δz) from the matrix surface to the migration front after 3 hours, or the number of cells at $\Delta z = 1$ mm after 12 hours of one representative experiment performed in triplicate ($n = 2$). *, $P < 0.05$; **, $P < 0.01$.

overcome by combining classical chemotherapy with matrix-degrading approaches, such as enzymatic degradation of hyaluronic acid (8, 36), drug stabilization and stromal depletion by nab-paclitaxel (6, 37) or the hedgehog signaling inhibitor IPI-926 (7, 38), or siRNA-mediated targeting of a collagen type I-specific chaperone in PSCs (39). A phase II clinical trial has already demonstrated beneficial effects of combinatorial therapy with gemcitabine and nab-paclitaxel on the survival of patients with pancreatic cancer (37).

We believe that the extensive desmoplasia in PDAC may also interfere with efficient endogenous antitumor T-cell responses, and may impede T-cell–based immunotherapeutic approaches. Hence, combining T-cell immunotherapy

(*Continued.*) Data are presented as the mean fluorescence intensity (MFI) and SD of seven (PBT$_{na}$ and PBT$_{a}$) or two (tumor-derived) independent experiments performed in triplicate. **, $P < 0.001$. C, migration of activated PBTs in a Boyden chamber in response to SDF-1 or IP-10, in the presence or absence of collagen type I coating, and with or without treatment with the anti–β_1-integrin blocking mAb. Data are shown as mean and SD of three independent experiments. D, migrational activity of activated PBTs and tumor-derived T cells with or without treatment with the anti–β_1-integrin blocking mAb, in a collagen type I matrix, in the presence of a chemokine gradient. The percentage of migrating cells/total cells is shown. Data show a representative experiment. E, directional migration of activated PBTs in a collagen type I matrix in the presence of a chemokine gradient. Colored lines represent individual cells. The percentage of cells oriented toward the chemokine-containing chamber ($= -\times$) is depicted. Combined data from two independent experiments are shown.

with matrix-degrading mechanisms might be a promising future treatment strategy. This approach could be improved further by strategies that redirect T cells toward their tumor cell targets. Therefore, there is a need to develop specific tools to target the contact guidance of T cells.

In summary, the excessive desmoplastic reaction in pancreatic cancer abrogates the chemokine-induced response of tumor-infiltrating T cells and switches their movement mode to contact guidance. The prevalence of contact guidance mediated by collagen fiber orientation along with the increased collagen density may jointly account for the stromal trapping of T cells observed in PDAC. These mechanisms may impede endogenous antitumor immune responses, and should be considered in the development of T-cell–based immunotherapies.

Disclosure of Potential Conflicts of Interest

No potential conflicts of interest were disclosed.

Authors' Contributions

Conception and design: E. Ryschich
Development of methodology: N. Hartmann, T. Giese, I. Poschke, E. Ryschich
Acquisition of data (provided animals, acquired and managed patients, provided facilities, etc.): N.A. Giese, T. Giese, R. Offringa, E. Ryschich
Analysis and interpretation of data (e.g., statistical analysis, biostatistics, computational analysis): N. Hartmann, T. Giese, E. Ryschich
Writing, review, and or revision of the manuscript: N. Hartmann, N.A. Giese, I. Poschke, R. Offringa, J. Werner, E. Ryschich
Administrative, technical, or material support (i.e., reporting or organizing data, constructing databases): N.A. Giese, I. Poschke, E. Ryschich
Study supervision: E. Ryschich

Acknowledgments

The authors thank Drs. N. Dross and C. Ackermann (Nikon Imaging Center, University of Heidelberg) for assisting with SHG microscopy and LSCM, Dr. W. Gross for help with cell tracking and statistical analysis, and C. Bernardi for excellent technical assistance.

Grant Support

The work was funded by Deutsche Forschungsgemeinschaft (to E. Ryschich; RY20/9-1).

The costs of publication of this article were defrayed in part by the payment of page charges. This article must therefore be hereby marked *advertisement* in accordance with 18 U.S.C. Section 1734 solely to indicate this fact.

Received October 29, 2013; revised March 20, 2014; accepted April 8, 2014; published OnlineFirst April 24, 2014.

References

1. Hidalgo M. Pancreatic cancer. N Engl J Med 2010;362:1605–17.
2. Neesse A, Michl P, Frese KK, Feig C, Cook N, Jacobetz MA, et al. Stromal biology and therapy in pancreatic cancer. Gut 2011;60:861–8.
3. Armstrong T, Packham G, Murphy LB, Bateman AC, Conti JA, Fine DR, et al. Type I collagen promotes the malignant phenotype of pancreatic ductal adenocarcinoma. Clin Cancer Res 2004;10:7427–37.
4. Mollenhauer J, Roether I, Kern HF. Distribution of extracellular matrix proteins in pancreatic ductal adenocarcinoma and its influence on tumor cell proliferation in vitro. Pancreas 1987;2:14–24.
5. Ryschich E, Khamidjanov A, Kerkadze V, Buchler MW, Zoller M, Schmidt J. Promotion of tumor cell migration by extracellular matrix proteins in human pancreatic cancer. Pancreas 2009;38:804–10.
6. Awasthi N, Zhang C, Schwarz AM, Hinz S, Wang C, Williams NS, et al. Comparative Benefits of Nab-paclitaxel over Gemcitabine or Polysorbate-based Docetaxel in Experimental Pancreatic Cancer. Carcinogenesis 2013;34:2361–9.
7. Olive KP, Jacobetz MA, Davidson CJ, Gopinathan A, McIntyre D, Honess D, et al. Inhibition of Hedgehog signaling enhances delivery of chemotherapy in a mouse model of pancreatic cancer. Science 2009;324:1457–61.
8. Provenzano PP, Cuevas C, Chang AE, Goel VK, Von Hoff DD, Hingorani SR. Enzymatic targeting of the stroma ablates physical barriers to treatment of pancreatic ductal adenocarcinoma. Cancer Cell 2012;21:418–29.
9. Fukunaga A, Miyamoto M, Cho Y, Murakami S, Kawarada Y, Oshikiri T, et al. CD8 +tumor-infiltrating lymphocytes together with CD4+ tumor-infiltrating lymphocytes and dendritic cells improve the prognosis of patients with pancreatic adenocarcinoma. Pancreas 2004;28:e26–31.
10. Ino Y, Yamazaki-Itoh R, Shimada K, Iwasaki M, Kosuge T, Kanai Y, et al. Immune cell infiltration as an indicator of the immune microenvironment of pancreatic cancer. Br J Cancer 2013;108:914–23.
11. Emmrich J, Weber I, Nausch M, Sparmann G, Koch K, Seyfarth M, et al. Immunohistochemical characterization of the pancreatic cellular infiltrate in normal pancreas, chronic pancreatitis and pancreatic carcinoma. Digestion 1998;59:192–8.
12. von Bernstorff W, Voss M, Freichel S, Schmid A, Vogel I, Johnk C, et al. Systemic and local immunosuppression in pancreatic cancer patients. Clin Cancer Res 2001;7:925s–32s.
13. Ryschich E, Notzel T, Hinz U, Autschbach F, Ferguson J, Simon I, et al. Control of T-cell-mediated immune response by HLA class I in human pancreatic carcinoma. Clin Cancer Res 2005;11:498–504.
14. Franciszkiewicz K, Boissonnas A, Boutet M, Combadiere C, Mami-Chouaib F. Role of chemokines and chemokine receptors in shaping the effector phase of the antitumor immune response. Cancer Res 2012;72:6325–32.
15. Friedl P, Weigelin B. Interstitial leukocyte migration and immune function. Nat Immunol 2008;9:960–9.
16. Bleul CC, Farzan M, Choe H, Parolin C, Clark-Lewis I, Sodroski J, et al. The lymphocyte chemoattractant SDF-1 is a ligand for LESTR/fusin and blocks HIV-1 entry. Nature 1996;382:829–33.
17. Loetscher M, Gerber B, Loetscher P, Jones SA, Piali L, Clark-Lewis I, et al. Chemokine receptor specific for IP10 and mig: structure, function, and expression in activated T-lymphocytes. J Exp Med 1996;184:963–9.
18. Raport CJ, Gosling J, Schweickart VL, Gray PW, Charo IF. Molecular cloning and functional characterization of a novel human CC chemokine receptor (CCR5) for RANTES, MIP-1beta, and MIP-1alpha. J Biol Chem 1996;271:17161–6.
19. Qin S, Rottman JB, Myers P, Kassam N, Weinblatt M, Loetscher M, et al. The chemokine receptors CXCR3 and CCR5 mark subsets of T cells associated with certain inflammatory reactions. J Clin Invest 1998;101:746–54.
20. Abastado JP. The next challenge in cancer immunotherapy: controlling T-cell traffic to the tumor. Cancer Res 2012;72:2159–61.
21. Oldham KA, Parsonage G, Bhatt RI, Wallace DM, Deshmukh N, Chaudhri S, et al. T lymphocyte recruitment into renal cell carcinoma tissue: a role for chemokine receptors CXCR3, CXCR6, CCR5, and CCR6. Eur Urol 2012;61:385–94.
22. Parsonage G, Machado LR, Hui JW, McLarnon A, Schmaler T, Balasothy M, et al. CXCR6 and CCR5 localize T lymphocyte subsets in nasopharyngeal carcinoma. Am J Pathol 2012;180:1215–22.
23. Friedl P, Brocker EB, Zanker KS. Integrins, cell matrix interactions and cell migration strategies: fundamental differences in leukocytes and tumor cells. Cell Adhes Commun 1998;6:225–36.
24. Wolf K, Friedl P. Extracellular matrix determinants of proteolytic and non-proteolytic cell migration. Trends Cell Biol 2011;21:736–44.

25. Ohno S, Tachibana M, Fujii T, Ueda S, Kubota H, Nagasue N. Role of stromal collagen in immunomodulation and prognosis of advanced gastric carcinoma. Int J Cancer 2002;97:770–4.
26. Peranzoni E, Rivas-Caicedo A, Bougherara H, Salmon H, Donnadieu E. Positive and negative influence of the matrix architecture on antitumor immune surveillance. Cell Mol Life Sci 2013;70:4431–48.
27. Salmon H, Franciszkiewicz K, Damotte D, Dieu-Nosjean MC, Validire P, Trautmann A, et al. Matrix architecture defines the preferential localization and migration of T cells into the stroma of human lung tumors. J Clin Invest 2012;122:899–910.
28. Bartel M, Hansch GM, Giese T, Penzel R, Ceyhan G, Ketterer K, et al. Abnormal crosstalk between pancreatic acini and macrophages during the clearance of apoptotic cells in chronic pancreatitis. J Pathol 2008;215:195–203.
29. Koninger J, Giese NA, Bartel M, di Mola FF, Berberat PO, di Sebastiano P, et al. The ECM proteoglycan decorin links desmoplasia and inflammation in chronic pancreatitis. J Clin Pathol 2006;59:21–7.
30. Ryschich E, Harms W, Loeffler T, Eble M, Klar E, Schmidt J. Radiation-induced leukocyte adhesion to endothelium in normal pancreas and in pancreatic carcinoma of the rat. Int J Cancer 2003;105:506–11.
31. Tharp WG, Yadav R, Irimia D, Upadhyaya A, Samadani A, Hurtado O, et al. Neutrophil chemorepulsion in defined interleukin-8 gradients in vitro and in vivo. J Leukoc Biol 2006;79:539–54.
32. Goldman R, Harvey J, Hogg N. VLA-2 is the integrin used as a collagen receptor by leukocytes. Eur J Immunol 1992;22:1109–14.
33. Hogg N, Henderson R, Leitinger B, McDowall A, Porter J, Stanley P. Mechanisms contributing to the activity of integrins on leukocytes. Immunol Rev 2002;186:164–71.
34. Wolf K, Muller R, Borgmann S, Brocker EB, Friedl P. Amoeboid shape change and contact guidance: T-lymphocyte crawling through fibrillar collagen is independent of matrix remodeling by MMPs and other proteases. Blood 2003;102:3262–9.
35. Wolf K, Te Lindert M, Krause M, Alexander S, Te Riet J, Willis AL, et al. Physical limits of cell migration: Control by ECM space and nuclear deformation and tuning by proteolysis and traction force. J Cell Biol 2013;201:1069–84.
36. Michl P, Gress TM. Improving drug delivery to pancreatic cancer: breaching the stromal fortress by targeting hyaluronic acid. Gut 2012;61:1377–9.
37. Von Hoff DD, Ramanathan RK, Borad MJ, Laheru DA, Smith LS, Wood TE, et al. Gemcitabine plus nab-paclitaxel is an active regimen in patients with advanced pancreatic cancer: a phase I/II trial. J Clin Oncol 2011;29:4548–54.
38. Cheng H, Merika E, Syrigos KN, Saif MW. Novel agents for the treatment of pancreatic adenocarcinoma. Highlights from the "2011 ASCO Annual Meeting". JOP 2011;12:334–8.
39. Ishiwatari H, Sato Y, Murase K, Yoneda A, Fujita R, Nishita H, et al. Treatment of pancreatic fibrosis with siRNA against a collagen-specific chaperone in vitamin A-coupled liposomes. Gut 2013;62:1328–39.